Vaporization of Ni, Al and Cr in Ni-Base Alloys and Its Influence on Surface Defect Formation During Manufacturing of Single-Crystal Components



Z.H. DONG, D. SERGEEV, D. KOBERTZ, N. D'SOUZA, S. FENG, M. MÜLLER, and H.B. DONG

Vaporization and its associated surface defect formation have become one of the most important challenges in manufacturing single-crystal components. During the kinetic-influenced casting and solution heat treatment of Ni-base superalloys, elements undergo processes of vaporization and deposition causing unpredictable defects. To quantitatively examine the vaporization phenomenon, partial vapor pressures of Ni, Al and Cr in Ni-base alloys were measured in the γ phase over the temperature range of 1473 K to 1650 K using Knudsen effusion mass spectrometry. Experimental results showed that the partial pressure of Al is about two orders of magnitude lower than that of Ni and five times lower than that of Cr, revealing that the vaporization of Al is almost negligible compared with those of Ni and Cr at solution heat treatment temperatures. Variation of partial pressures during homogenization of the as-cast Ni-base alloys was measured in long-term isothermal experiments at 1573 K. It was found that Cr vapor pressure decreases by a factor of two in the first 20 hours whereas the Ni and Al remain nearly constant.

https://doi.org/10.1007/s11661-019-05498-1 © The Author(s) 2019

I. INTRODUCTION

NI-BASE superalloys have been developed for high-temperature applications owing to their exceptional high-temperature capability. [1-3] A high-level content of alloying elements has been used to improve creep strength in recent generations of Ni-base single-crystal superalloys, such as CMSX-10, [4-8] for turbine blades with the introduction of refractory elements. [9-11] However, the additional content in new alloys caused severe solidification segregation that eventually promoted the presence of casting defects. [12-19] In addition, due to the preferential partitioning and slow diffusivity of refractory elements in Ni-base superalloys, further heat treatment for refractory-containing superalloys often required a longer time and higher temperature solution heat treatments to dissolve the inter-dendritic eutectic phase and homogenize the microstructure. For example, solutioning of as-cast CMSX-10 turbine blades was carried out above

Knudsen effusion mass spectrometry (KEMS) has been used to measure the vapor species and their equilibrium pressure above the condensed phase at high temperatures. It is a novel method that offers the highest accuracy for vaporization studies under equilibrium^[32–34] providing direct evidence in terms of thermodynamics. Although thermodynamic activities of

Manuscript submitted August 7, 2018. Article published online October 16, 2019

the γ' solvus temperature of around 1473 K to 1633 K for a total of approximately 45 hours. [20–25] Time-consuming heat treatment generates certain challenges and costs in superalloy production. As a result, recent studies revealed that vaporization of Ni, Al and Cr occurs during solution heat treatment, which leads to the formation of various surface defects, such as surface recrystallization, surface scale and melting during manufacturing. [26-28] Vaporization-induced surface defects in Ni-base superalloys have become one of the most important challenges in manufacturing single-crystal components.^[28–30] Due to the important roles of Ni, Al and Cr affecting vaporization during solution heat treatment of Ni-base superalloys revealed by our previous publication, [27,28,31] Ni-Al-Cr alloys were selected for vaporization examination of their thermodynamic properties for simplicity purposes. To understand the mechanism and minimize the surface defect formation during manufacturing of Ni-base superalloys, we conducted quantitative analysis of elemental vaporization under real industrial processing conditions.

Z.H. DONG, S. FENG, and H.B. DONG are with the Department of Engineering, University of Leicester, Leicester LE1 7RH, UK. Contact e-mail: hd38@le.ac.uk D. SERGEEV, D. KOBERTZ, and M. MÜLLER are with the Forschungszentrum Jülich GmbH, IEK-2, Leo-Brandt-Str.1, 52425, Jülich, Germany. N. D'SOUZA is with the Rolls-Royce plc, P.O. Box 31, Derby DE24 8BJ, UK.

some elements in Ni-base alloys have been measured using KEMS, [35-42] there are insufficient data for examining Ni-base alloys with concentrations from modern designs. Correlation between elemental vaporization at solutioning temperature and elemental interaction with respect to phase evolution has not yet been properly assessed and justified in this alloying system. In this study, we used the KEMS method to measure the partial pressures of Ni, Al and Cr in Ni-base alloys at an industrial heat treatment temperature range from 1473 K to 1650 K; accurate partial pressure data are obtained and used to analyze surface defect formation during manufacturing. Our results provide an insight into the mechanism of surface defect formation and can be used to optimize the industrial heat treatment process to reduce kinetic-orientated surface defects.

II. EXPERIMENTS

A. Sample Preparation

Polycrystalline Ni-Al-Cr alloy samples were made from high-purity Ni (99.99 pct), Cr (99.98 pct) and Al (99.99 pct), supplied by Trillion Metals Co., Ltd., in the preparation of test bars by rapid vacuum melting. Raw material was prepared and weighted to an accuracy of 0.001 g prior to the casting stage, which was carried out in a vacuum induction levitation melting furnace. A mixture of raw material was heated by induction to a temperature of about 1723 K in the furnace while levitating in a magnetic field. The whole process operated in the condition of a vacuum level at 0.1 Pa and lasted for approximately 15 minutes until the alloy was fully melted with a uniform chemistry in the furnace. The molten alloy was then pressed into a fused quartz tube at an approximate rate of 0.05 m/s to form a cylindrical bar, which was subsequently quenched by Ar flow. Rapid solidification prevents alloys from macro-segregation in as-cast microstructure. The quartz tube was then removed from the produced sample bar, which has a length of approximately 150 mm and diameter of 8 mm after casting.

Five Ni-Al-Cr alloys were designed with constant Al content (12 at. pct), which is similar to the Al concentration in commercial single-crystal alloy CMSX series, and the content of Cr increases from 2 to 30 at. pct. Compositions of model alloys used in KEMS experiments are listed in Table I and were ascertained by inductively coupled plasma mass spectrometry. All alloys are consistent with nominal compositions in the original design, implying no significant loss by vaporization during the production process.

The calculated isothermal section for the Al-Ni-Cr system at 1573 K compared with the experimental points is presented in Figure 1. The ternary phase diagram is adapted from the optimized plot by Velikanova *et al.*^[43] with respect to the original work from Dupin *et al.*^[44] All model alloys used in this study are labeled in Figure 1 showing a single phase of Ni-Cr-Al alloys produced at 1573 K within the γ phase (FCC_A1) region. Despite the different phase diagram

predicted from the FactSage thermochemical software package program^[45] implemented with the SGTE 2017 database (Intermetallic Compounds, Alloy Solutions), it is also noteworthy that KEMS data enable correction of the existing phase diagram *via* thermodynamic analysis with great detail.

B. Knudsen Effusion Mass Spectrometry

The measurements of partial vapor pressures of Ni, Al and Cr in Ni-Al-Cr alloys were conducted using a Knudsen effusion mass spectrometer at Forschungszentrum Jülich in Germany. A single-focusing CH5 (Finnigan MAT 271, Bremen) 90 deg magnetic sector-field mass spectrometer was used.

As illustrated in Figure 2, the sample is held in the Knudsen cell and heated uniformly. A molecular beam of evaporated species from the Knudsen cell enters the ion source via an aperture. The shutter is used to separate the ion source from the sample chamber controlling the intensity of the formed beam. The vapor species are ionized by electron impact $[M (g) + e^{-} =$ M⁺ + 2e⁻) by an emission current of 0.5 mA and electron energy of 70 eV. A set of collimating lenses focuses the ion beam, and, on the way to the entrance slit of the mass analyzer, the ion kinetic energy is boosted by an accelerating potential of 8 kV. The entering kinetic energy of all ions with the same charge is nearly mono-energetic at 8 keV, but their velocities follow the law of classical mechanics, wherein the speed of a particular ion is proportional to the reciprocal to the square root of its mass. When an ion passes the sector field analyzer, its path is influenced by a combined action of perpendicular electric and magnetic fields described by the electromagnetic force. By dynamically changing the electrical field strength, the ions of different mass are separated according to their mass-to-charge ratio. The separated ions are collected in the detector for final evaluation. A quantity of ions is directed into a Faraday cage, and the current is directly recorded as a potential drop across a high resistance ($10^{11} \Omega$). At low quantity, the ions are directed to impact the first dynode of the multiplier, where they induce a secondary emission of electrons. The secondary electrons are amplified through a cascade of plates with increasing potential difference. On each plate the electron emission is multiplied, and finally the number of secondary electrons ends in a shower that is about 10⁶ times the starting number. The number of electrons is now high enough to be recorded as either a potential drop through a resistor or a burst that is counted (ion counting). In this study, all experiments were generally completed with ion counting to avoid a mass discrimination caused by the multiplier. An intensity signal of a potential drop was obtained by conversion of the ion counts. [47]

In our experiments, an Al_2O_3 crucible inside the iridium Knudsen cell with a diameter of 9 mm and an orifice size of 0.3 mm was used to prevent chemical reaction with Ir. Thermal isolation of the Knudsen cell was achieved by using tantalum radiation shields during measurements. The cell was heated by electron bombardment at a potential 1200 V and a variation of the

Table I. Compositional Change (At. Pct) of Ni-Al-Cr Alloys Before and After KEMS Experiments

	Ni		C	r	Al		
Alloy (At. Pct)	Before	After	Before	After	Before	After	
Ni2Cr12Al	85.71	85.73	2.17	1.13	12.12	13.14	
Ni5Cr12Al	83.19	84.57	5.15	2.45	11.66	12.98	
Ni15Cr12Al	72.62	77.56	15.43	9.23	11.95	13.21	
Ni20Cr12A1	67.96	71.28	20.42	16.61	11.62	12.11	
Ni30Cr12Al	58.71	64.25	29.68	24.36	11.61	11.39	

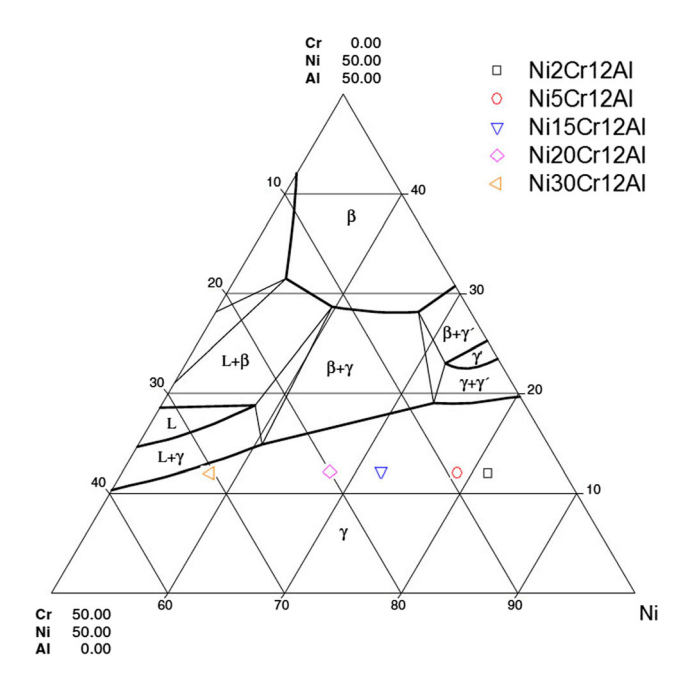


Fig. 1—Ternary diagram of Ni-Al-Cr alloys with labels of measured alloys for KEMS experiments showing present phase at 1573 K.^[45]

electron emission related to the temperature under consideration. The temperature at the bottom of the Knudsen cell was measured by an optical pyrometer (Dr. Georg Maurer GmbH, Kohlberg, Germany) in a black body hole at the bottom of the cylindrical Knudsen cell. The pyrometer was calibrated by the melting points of Ag, Au, Ni and Pt. To distinguish the signal out of the cell from the background, a movable shutter allows suppressing the beam before the ion source. The accurate control of temperature, Knudsen cell geometry and other relevant parameters of measuring ion intensity in different experiments ensures the reliability of measured results for subsequent partial pressure calculations.

Samples were placed inside a cylindrical crucible (ϕ 5 mm, height of 3 mm) with an approximate weight range from 50 to 100 mg. Each sample was weighted at an accuracy of 0.1 mg. All designed alloys were initially measured using heating and cooling cycles at a desired temperature range. After reaching the setup temperature, the program waits until the ion signal is constant (about 8 to 10 minutes for alloys). A constant signal indicates chemical equilibrium, *i.e.*, constant chemical

potential. Once a constant signal has been confirmed, measurements of Ni, Al and Cr were recorded in shutter open and close conditions, labeled as (O) and (C). The time to register one ion depends on the sampling rate (about 20 s/ion). It took roughly 2 minutes for a single measurement, so a set of six measurements at a sequence of Ni(O), Ni(C), Cr(O), Cr(C), Al(O) and Al(C) took 12 minutes at one temperature. The time interval for temperature change was set to about 8 minutes waiting for signal constants. Samples were heated/cooled with repetition at 20-K intervals between 1473 K and 1650 K depending on the liquidus of alloys^[48] (also see Appendix Table A1).

In situ isothermal holds (solution heat treatment) were carried out from 60 to 114 hours to determine the extent of elemental vaporization continuously. For comparison, the extent of element vaporization in these experiments was determined using the ion intensity change by KEMS.

III. EQUATIONS FOR CALCULATING PARTIAL PRESSURE AND THERMODYNAMIC ACTIVITY

Thermodynamic equilibrium is assumed in a closed system during KEMS measurements while a small fraction of molecules (< 1 mg in 24 hours) effuses from a tiny orifice on top of the Knudsen cell. [34,49,50] A long isothermal session is needed to effuse composition changing amounts. The vaporization of Ni, Al and Cr elements was detected by counting Ni⁺, Al⁺ and Cr⁺ ions from gaseous species M (g) (M = Ni, Al, Cr) originating from the Knudsen cell with a reaction equation as: M (g) + $e^- = M^+ + 2e^-$.

The method for evaluating partial pressure and activity has been well described by Hilpert^[32] and Kobertz *et al.*^[47] The relevant evaluation of the ion-current-ratio technique can be found in the work of Neckel and Wagner^[51] and Belton and Fruehan.^[52] Using the method in References 32 and 47, partial pressure is determined from measured ion intensities I_i of species i at temperature T using Eq. [1]:

$$p_i = k \frac{I_i T}{\sigma_i \gamma_i \eta_i},$$
 [1]

where T is the temperature in Kelvin, k is the pressure calibration factor, p_i denotes the partial pressure, σ_i is the ionization cross section, and η_i is the isotopic

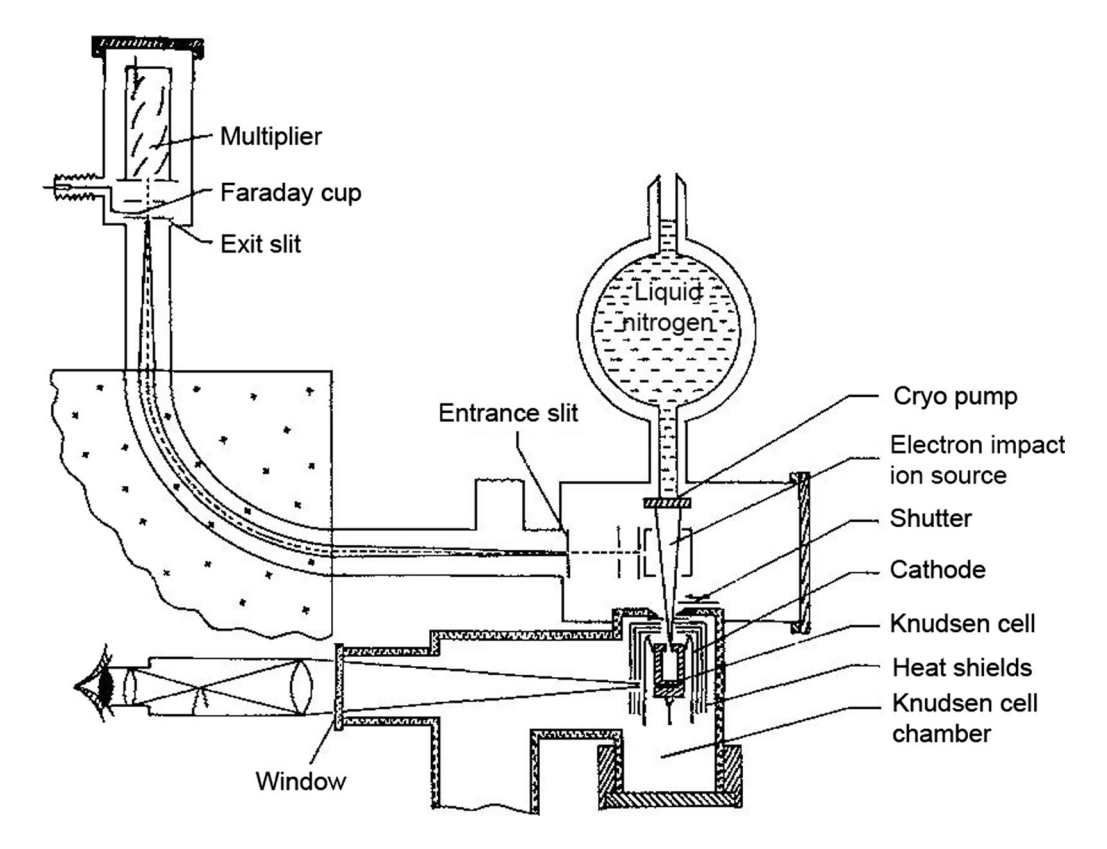


Fig. 2—Schematic setup of a magnetic sector-field Knudsen effusion mass spectrometer. Adapted from Ref. [46] with permission of the Electrochemical Society, Inc.

abundance of species *i*. The coefficient γ_i is the multiplier factor, which is unity for an ion-counting system.

The ionization cross sections used for the gaseous species are $\sigma_{\rm Ni}=5.48,~\sigma_{\rm Al}=6.18$ and $\sigma_{\rm Cr}=5.1,$ which were reported by Mann *et al.*^[53] at an ionization energy of 70 eV. The isotopic abundance of Ni and Cr was normalized to 100 pct corresponding to the mass of their most abundant isotopes, *i.e.*, Ni⁵⁸ and Cr⁵², calculated as $\eta_{\rm Ni}=0.682$ and $\eta_{\rm Cr}=0.838$, while Al²⁷ has a natural abundance of 100 pct giving the only isotope for Al with $\eta_{\rm Al}=1.^{[54-56]}$

The pressure calibration factor can be derived by comparing the vapor pressure of pure Ni, Al and Cr calculated from KEMS measurements with that of reference from IVTANTHERMO data. Therefore, by re-arranging Eq. [1], the calibration factor for Ni is given by $2.71 \times 10^{-9} \text{ Pa/mV K}$ using values of $p_{\text{Ni}} = 8.44 \times 10^{-3} \text{ Pa}, [57] \eta(\text{Ni}) = 0.682, \sigma(\text{Ni}) = 5.48$ and $I_{\text{Ni}}T = 1.15 \times 10^7 \text{ mV K}$. Pressure calibration factors for Cr and Al can be calculated in the same manner

After calibration of pressure factor k, partial pressures of Ni, Al and Cr are calculated from measured ion intensities of elements from Eq. [1]. According to the Clausius–Clapeyron equation, [58,59] the partial pressure for the standard condition is set to conditions at T=298 K and $p=1 \text{ atm}=p^{\Theta}$. Hence, the activity a_i of a species is calculated in the partial pressure of the element in a measured alloy compared with the standard pressure, p^{Θ} , which is listed as Eq. [2]:

$$a_i = \frac{p_i}{p^{\Theta}} / \frac{p_i^0}{p^{\Theta}} = \frac{p_i}{p_i^0},$$
 [2]

where p_i and p_i^0 are the equilibrium vapor pressure of i over the alloy and pure substance at the same temperature, respectively.

The equilibrium constant K is defined as the product of the activities a_i of the reactants, which can be determined from partial pressures and temperature dependence^[32] using Eq. [3]:

$$K_{\rm p} = \Pi \left(\frac{p_i}{p^{\Theta}} \right). \tag{3}$$

Considering the KEMS method, for a pure element, partial pressure using Eq. [1] can be arranged as Eq. [4]:

$$p_{\rm p} = k \frac{I_{\rm p} T}{\sigma_{\rm p} \gamma_{\rm p} \eta_{\rm p}}.$$
 [4]

For a system, the partial pressure in Eq. [1] is shown as follows:

$$p_{\rm s} = k \frac{I_{\rm s} T}{\sigma_{\rm s} \gamma_{\rm s} \eta_{\rm s}}.$$
 [5]

It is considered in the same element, $\sigma_{\rm p}=\sigma_{\rm s},~_{\rm p}=_{\rm s},~_{\rm p}=_{\rm s},~_{\rm p}=_{\rm s},~_{\rm p}=_{\rm s}$; therefore, activity can now be calculated using

the following equation with values at the same temperature:

$$a = \frac{p_{\rm s}}{p_{\rm p}} = \frac{I_{\rm s}}{I_{\rm p}}.$$
 [6]

As $\Delta G = 0$ in equilibrium, the Gibbs energy is derived with respect to the equilibrium constant K_p according to its definition as:

$$\Delta G_{\rm T}^0 = -RT \ln K_{\rm p} = \Delta_{\rm sub} H_i^0 - T \Delta_{\rm sub} S_i^0.$$
 [7]

Thus, the equilibrium constant K_p is determined as an Arrhenius plot by rearranging Eq. [7]:

$$\ln K_{\rm p} = -\frac{\Delta_{\rm sub} H_i^0}{R} \frac{1}{T} + \frac{\Delta_{\rm sub} S_i^0}{R}.$$
 [8]

 $\Delta_{\mathrm{sub}}H_i^0$ is the enthalpy of vaporization for species i, and $\Delta_{\mathrm{sub}}S_i^0$ is the entropy of vaporization for species i. R is the gas constant. In the equation, the ratio of $\Delta_{\mathrm{sub}}H_i^0$ and $\Delta_{\mathrm{sub}}S_i^0$ to the gas constant can be presented as constants A and B; therefore, the linearity logarithm of the partial pressure and reciprocal temperatures is obtained.

Considering the reaction for element i in the condensed phase and gas phase as the following reaction $i(c) \rightleftharpoons i(g)$, K_p in the pure element becomes:

$$K_{\rm p}(i)_{\rm p} = \frac{p_{\rm p}(i({\rm g}))}{a_{\rm p}(i({\rm c}))} = p_{\rm p}(i({\rm g}))$$
 [9]

where activity for the pure element is equal to 1.

Following the same principle, K_p for a system is presented as Eq. [10]:

$$K_{\rm p}(i)_{\rm s} = \frac{p_{\rm s}(i({\rm g}))}{a(i({\rm c}))}.$$
 [10]

Combining Eqs. [9] and [10], the activity of element i in the system is derived as:

$$a(i) = \frac{p_s(i(g))}{p_p(i(g))}.$$
 [11]

The Arrhenius plot in Eq. [8] is rearranged with respect to Eq. [3] in terms of the activity against reciprocal temperature as:

$$\ln\left(\frac{p_{s}}{p_{p}}\right) = \ln a_{i} = -\frac{\Delta_{s}H_{i}^{0}}{R}\frac{1}{T} + \frac{\Delta_{s}S_{i}^{0}}{R} = -A\frac{1}{T} + B. \quad [12]$$

IV. RESULTS

In this section the partial pressures of Ni, Al and Cr in pure substance and alloys will be reported first, followed by the derived chemical potential of Ni, Al and Cr as supportive evidence for interpreting the phenomenon of elemental vaporization at high temperatures. Results from isothermal experiments further revealed the extent of elemental change during solution heat treatment. Finally, implications from the current study are discussed to establish the understanding of elemental interaction during processing of Ni-base superalloys.

A. Sublimation Enthalpy and Entropy of Pure Ni, Al and Cr

As described in the Section II, upon vaporization, ions of Ni⁺, Cr⁺ and Al⁺ were collected separately from gaseous species, and the number of ions was counted by a digital impulse counter. For Ni and Cr, the ion intensity peaks were measured and normalized to 100 pct corresponding to the mass of their most abundance isotopes, *i.e.*, Ni⁵⁸ and Cr⁵², while Al²⁷ has a natural abundance of 100 pct giving the only isotope for Al.^[54–56] The ionization cross sections used for the gaseous species were collected from Mann's study proving production of ion intensity and temperature (IT) normalized by the abundance and ionization cross section.

Figure 3 depicts the natural logarithm of normalized (IT) for the measured elements of Ni, Al and Cr against reciprocal temperature. The linearity of Arrhenius lines indicates that measurements of ion intensity in our experiments were stable, and therefore a steady-state condition was satisfied during the experiments. With application of the principal calculation described above, normalized (IT) can be converted into partial pressures as subsequent results.

Reliability of KEMS measurements is further examined by comparing enthalpies of sublimation from our experiments with those in the literature. Coefficients A and B from the Arrhenius plot, derived as $\ln(p_i) = -A/T + B$, were used to calculate the enthalpy and entropy

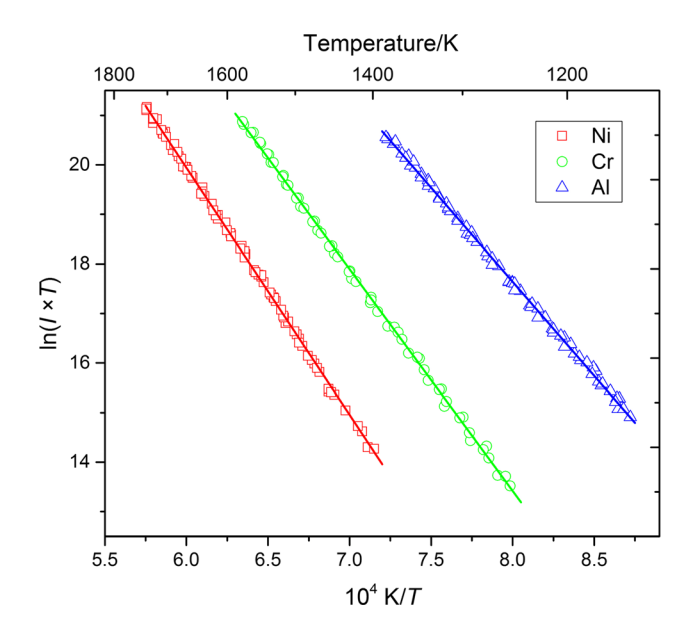


Fig. 3—Arrhenius plot of $ln(I \times T)$ vs the reciprocal absolute temperature (1/T) from KEMS measurements of three pure substances.

Table II. Partial Pressure Equation $\ln(p) = -A/T + B$ of Measured Pure Ni, Al and Cr and Their Enthalpy of Sublimation $(\Delta_{\text{sub}} H_{\text{Tm}} = -A \times R)$ and Entropy $(\Delta_{\text{sub}} S_{\text{Tm}} = B \times R)$ at Mean Temperature T_{m}/K

	Temperature Range (K)	Mean Temp. $T_{\rm m}$ (K)	$A/10^4$	В	$\Delta_{\text{sub}}H_{\text{Tm}}$ (kJ/mol)	$\Delta_{sub}S_{Tm}$ (J/(mol K)	$\Delta_{\rm ref} H^{[29]} \ ({\rm kJ/mol})$
Ni	1423–1750	1587	3.734	28.451	414.3	236.4	414.5 ± 0.2
Al	1150–1400	1275		24.998	310.3	207.7	310.2 ± 3.2
Cr	1250–1573	1412		27.872	383.3	231.6	384.3 ± 1.0

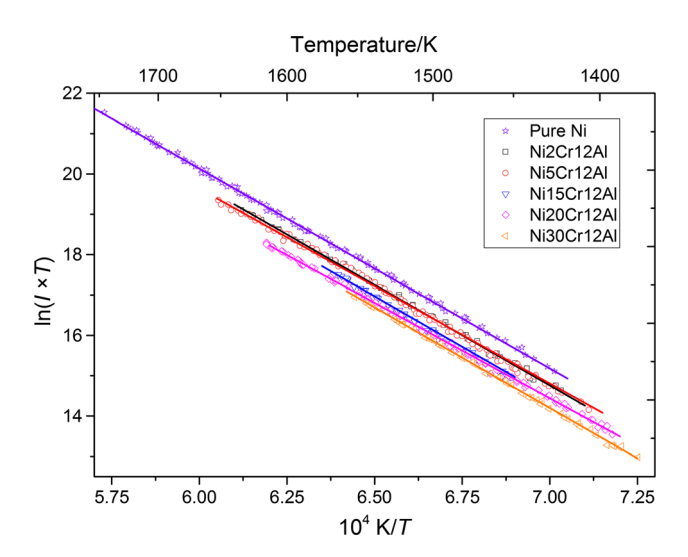


Fig. 4—Arrhenius plot of $\ln(I \times T)$ vs the reciprocal absolute temperature (1/T) for pure Ni and Ni in measured Ni-Al-Cr alloys producing regression equations as thermodynamic descriptions (second law determination).

of sublimation as $\Delta_{\text{sub}}H_i(T) = -A \times R$ and $\Delta_{\text{sub}}S_i(T) = -B \times R$, with R = 8.314 J/mol/K.

All enthalpies and entropies of sublimation from our measurements and literature data^[57,60] are listed in Table II. The enthalpy changes from our measurements at mean temperature of the measured range are $\Delta_{\rm sub}H_{\rm Ni}$ (1562 K) = 414.26 \pm 0.3 kJ/mol, $\Delta_{\rm sub}H_{\rm Cr}$ (1476 K) = 383.3 \pm 3.2 kJ/mol and $\Delta_{\rm sub}H_{\rm Al}$ (1284 K) = 310.3 \pm 1.9 kJ/mol, respectively. The literature data from the IVTANTHERMO database^[57] are: $\Delta_{\rm sub}H_{\rm Ni}$ (1500.5 K) = 414.5 kJ/mol, $\Delta_{\rm sub}H_{\rm Cr}$ (1523 K) = 384.3 kJ/mol, $\Delta_{\rm sub}H_{\rm Al}$ (1323 K) = 310.2 kJ/mol, showing good agreement obtained between our measurements and data from the literature.

B. Partial Vapor Pressures of Ni, Al and Cr in Ni-Al-Cr Alloys

In this section, the equations for calculating the vapor partial pressure will be presented first, and then the temperature and composition dependence of the partial vapor pressures will be reported. It shall be pointed out that only a single γ phase exists in all the experimental Ni-Al-Cr alloys from 1473 K to 1650 K, as predicted in Figure 1, and our KEMS results on Ni activity νs Ni contents will be reported in Section IV–C.

1. Equations for calculating partial vapor pressures of Ni, Al and Cr in Ni-Al-Cr alloys

Figure 4 contains the calculated ln(IT) against $10^4/T$ from measured Ni data of pure Ni and that of Ni-Al-Cr alloys. As expected, the magnitude of ln(IT) shows direct proportion to the Ni concentration. The partial vapor pressure of the alloy elements as a function of the temperature $(p_i = f(T))$ can be deduced from the Arrhenius plot in the form of a linear function $ln(p_i) =$ A/T + B. Two independent runs were carried out, and the regression performed on the two runs is presented as an equation with an appropriate uncertainty. The deviations of scatter plots are eliminated statistically by using the Grubbs outlier method. [61] With application of the same principle, derived equations for calculating the partial vapor pressure of Al and Cr in Ni-Al-Cr alloys are also listed in Table III. All partial vapor pressures were calculated in Pa.

2. Temperature dependence

Figure 5 shows partial vapor pressures of Ni, Al and Cr calculated from measured ion intensities in the Ni2Cr12Al alloy. Partial vapor pressures of Ni, labeled as square dots in Figure 5, increase from 0.0012 to 0.12 Pa between 1424 K to 1636 K; triangle dots showing partial vapor pressure for Al ascend by nearly two orders of magnitude from 8.13×10^{-6} Pa at 1424 K to 9.9×10^{-4} Pa at 1636 K. Circle dots for partial vapor pressure of Cr also show a significant increase within an extensive range of magnitude at elevated temperatures, from 4.51×10^{-5} Pa at 1436 K to 0.0018 Pa at 1636 K, despite a lower increasing rate. All three partial pressures in Ni-Cr-Al alloys show a great dependence of temperature. The rest of the measured Ni-Al-Cr alloys show a similar pattern for temperature dependence, and the measured temperature range depends on their solidus temperatures, which are lowered by the amount of additions contained in the alloys. Therefore, the order of magnitude of three partial pressures in the measured Ni-Al-Cr alloys is obtained as P Ni > P Cr > P Al. Additional details of Cr vaporization can be further observed in isothermal experiments showing consistency in terms of the decrease of Cr concentration in the measured alloys.

3. Composition dependence

As partial vapor pressures of Ni, Al and Cr have been measured in five Ni-Al-Cr alloys with different compositions in our KEMS experiments, the relationship between partial vapor pressure and compositions was

Table III. Partial Pressure (Pa) Equation, $\ln(p_i) = -A \frac{\pi}{1} + B$, of Ni, Al and Cr in Ni-Al-Cr Alloys as a Function of Temperatures

					$\ln(p_i) =$	$\ln(p_i) = -A\frac{1}{T} + B$		
			I	Ņ)	$\Im {f r}$	4	יו
Alloy Composition	Temperature (K)		$A/10^{4}$	В	$A/10^4$	В	$A/10^4$	В
		run 1	4.986 ± 0.08	28.257 ± 0.03	4.277 ± 0.01	19.842 ± 0.05	5.169 ± 0.04	24.774 ± 0.22
Ni2Cr12A1	1423–1636	run 2	4.976 ± 0.06	28.105 ± 0.03	4.265 ± 0.01	19.679 ± 0.03	5.254 ± 0.02	25.229 ± 0.08
		regression	4.997 ± 0.08	28.289 ± 0.04	4.281 ± 0.02	19.826 ± 0.07	5.271 ± 0.02	25.375 ± 0.14
		run 1	4.916 ± 0.04	#	4.294 ± 0.03	+	5.224 ± 0.03	25.14 ± 0.12
Ni5Cr12A1	1372–1651	run 2	4.908 ± 0.02	+	+	20.652 ± 0.11	+	25.178 ± 0.08
		regression	4.907 ± 0.04	Н	#	+	+	25.121 ± 0.11
		run 1	4.989 ± 0.03	+	+	+	+	+
Ni15Cr12Al	1445–1652	run 2	4.981 ± 0.02	27.943 ± 0.06	4.222 ± 0.03	22.87 ± 0.18	5.302 ± 0.04	26.165 ± 0.02
		regression	4.964 ± 0.06	Н	+	#	+	+
		run 1	4.913 ± 0.07	Н	#	#	+	+
Ni20Cr12Al	1368–1616	run 2	4.896 ± 0.04	Н	#	#	+	+
		regression	4.943 ± 0.05	Н	#	#	+	24.925 ± 0.07
		run 1	5.012 ± 0.03	Н	#	4	4.826 ± 0.01	24.417 ± 0.03
Ni30Cr12Al	1375–1598	run 2	4.952 ± 0.01	27.471 ± 0.02	+	23.957 ± 0.13	4.833 ± 0.01	24.487 ± 0.01
		regression	4.984 ± 0.02	27.682 ± 0.01	+	+1	+	24.516 ± 0.02

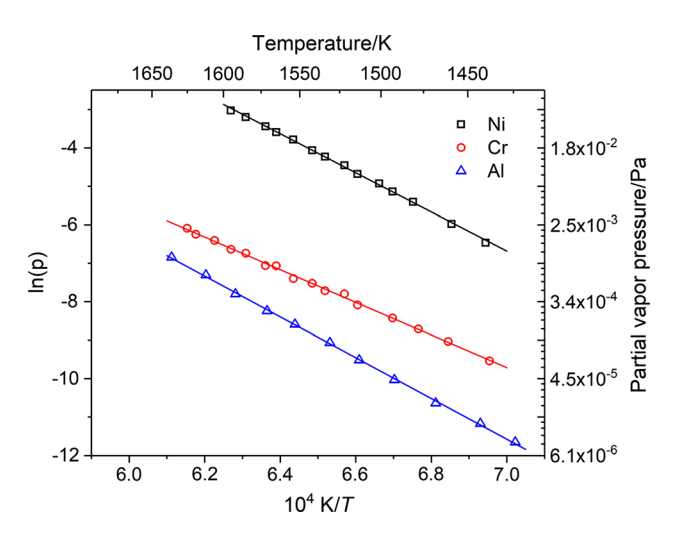


Fig. 5—Temperature dependence of partial vapor pressure (Pa) of Ni, Al and Cr in the Ni2Cr12Al alloy.

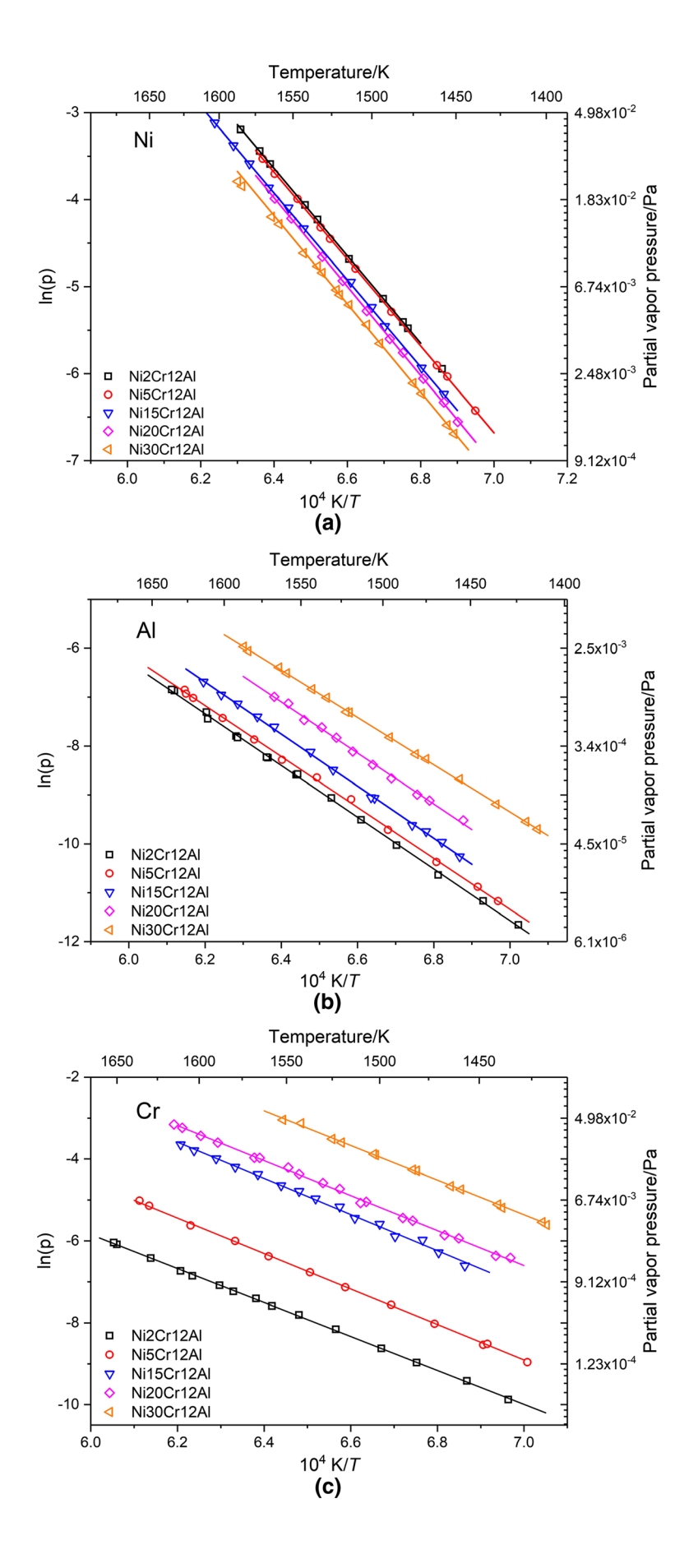
analyzed, and the results of partial vapor pressures for the five alloys with different Cr concentrations are shown in Figure 6. Partial vapor pressures of Ni and Al, as shown in Figures 6(a) and (b), respectively, in Ni-Al-Cr alloys are directly proportional to elemental concentrations as higher content of elements in alloy contributes to an increased partial vapor pressure. Presumably, nickel is the major element in the alloy, and the partial pressure of Ni is dominant. The partial vapor pressure of Cr increases when an additional amount of it is added to the alloy. As depicted in Figure 6(c), the partial vapor pressure of Cr changes from 2.86×10^{-4} Pa for Ni2Cr12Al alloy to 0.028 Pa from Ni3OCr12Al alloy at 1523 K.

Despite a constant constitution of about 12 at. pct of Al in all Ni-Al-Cr alloys, the partial vapor pressure of Al shows an increase with the addition of Cr content in alloys, which changed from 9.3×10^{-5} Pa for Ni2Cr12Al alloys to 6.7×10^{-4} Pa for Ni30Cr12Al alloys at 1523 K.

C. Thermodynamic Properties of Ni, Al and Cr in Ni-Al-Cr Alloys

In addition, the enthalpy and entropy of sublimation for individual elements in Ni-Al-Cr alloys can be obtained using coefficients A and B listed in Table III with the method described above. Table IV summarizes the enthalpy and entropy of sublimation for individual elements in all measured Ni-Al-Cr alloys. The data reveal that entropies of sublimation for Ni and Al fluctuate in a slight range with different concentrations in alloys, while the entropy of sublimation for Cr varies with an increasing concentration. Therefore, it can be concluded that the sublimation of different alloys is driven by the entropy of Cr in the Ni-Al-Cr system.

KEMS data are naturally calculated as thermodynamic activity to reveal the interaction and stability in the condensed phase, which is referred to the solid state of elements in all measured Ni-Al-Cr alloys. Experimental activities of Ni, Al and Cr are plotted as $\ln(a)$ vs



◆Fig. 6—Partial vapor pressures (Pa) of (a) Ni, (b) Al and (c) Cr as a function of the inverse absolute temperature (1/T) in all Ni-Al-Cr alloys showing composition dependence in measured alloys.

1/T in Figure 7 with the regression equation of $\ln(a) = -A\frac{1}{T} + B$ from linearity fitting. Good reproducibility of KEMS results was obtained from multiple runs of experiments performed on Ni-Al-Cr alloys. Coefficients of A and B from the Arrhenius plot of all measured Ni-Al-Cr alloys are listed in Table V providing assessment of the thermodynamic activities of Ni, Al and Cr at any desired temperatures.

Apart from the partial pressure and thermodynamic activity presented above, there is more information that can be derived from KEMS data by considering the correlation to compositions of alloys. As illustrated in Figure 8, partial vapor pressures of Ni are plotted as a function of the equivalent mole fraction to determine their ideality to Raoult's law for the measured Ni-Al-Cr alloys, and the possibility of phase transitions occurs during heat treatment; Figure 9 plots those of Cr in the same manner. Both figures contain vapor pressures of Ni and Cr with respect to the ideal Raoult's law as a comparison to KEMS data. The results were evaluated at 1473 K and 1573 K showing partial pressures for Ni and Cr in Ni-Al-Cr alloys both negatively deviate from ideality to Raoult's law at different temperatures.

Based on the phase rule, $\mathrm{Ni}^+/\mathrm{Al}^+$ ion intensity ratios are independent of concentration x_{Ni} if three phases are present in the ternary alloy system at the measured temperatures. Hence, it is deduced that the partial pressure or thermodynamic activity remains at a constant level when the phase transition occurs because of the direct proportionality of partial pressure with respect to ion intensity.

D. Elemental Vaporization During Real Industrial Heat Treatment Processes

As described in the Section II, in situ isothermal hold was performed at 1573 K for Ni2Cr12Al, Ni5Cr12Al and Ni15Cr12Al alloys from 66 to 114 hours for inspection of variation in ion intensity. The measured ion intensity and calculated partial vapor pressure of Cr

in Ni2Cr12Al alloy are presented in Figure 10. It is observed that there is an initial decline of both ion intensity and partial vapor pressure in the first 20 hours; the partial vapor pressure changed from 2.57×10^{-3} Pa at the beginning to 1.39×10^{-3} Pa at 20 hours. As shown in Figure 10(a), the process of stabilization observed for the partial vapor pressure of Ni after 20 hours remained around 0.035 Pa. Partial vapor pressure of Cr stabilizes at a level of 1.02×10^{-3} Pa with small fluctuations after the initial decline over about 20 hours in Figure 10(b). To confirm the effect of elemental variations on vaporization and equilibration among Ni-Al-Cr alloys, the ratios of ion intensity are presented as Cr/Ni and Al/Ni for three measured alloys over the initial period in the illustration in Figure 11. In Figure 11(a), the Cr/Ni ratio descends by a factor of 2 in first 20 hours. Figure 11(b) shows that the Al/Ni ratio remains stable during isothermal hold. The ratio of ion intensity change from the isothermal hold suggests that the concentration change of Cr, regarding changing the chemical potential, is the main reason for the ion intensity decline during the initial period of isothermal hold. On the other hand, the results show a homogenization of the non-equilibrium state of as-cast samples

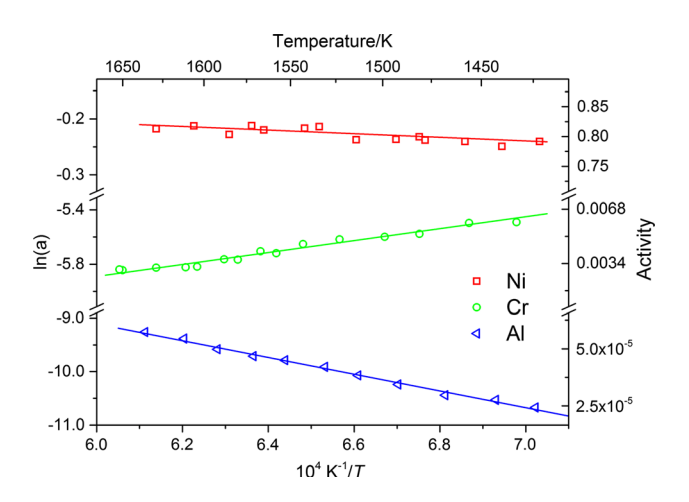


Fig. 7—Thermodynamic activity of Ni, Al and Cr as a function of the inverse absolute temperature (1/T) in Ni-2Cr-12Al alloys.

Table IV. Sublimation Enthalpy and Entropy for Measured Ni-Al-Cr Alloys

	Enthalpy and Entropy of Sublimation						
	Ni		(Cr	Al		
Alloy Composition	H (kJ/mol)	S (J/(mol K)	H (kJ/mol)	S (J/(mol K)	H (kJ/mol)	S (J/(mol K)	
Ni-2Cr-12Al Ni-5Cr-12Al Ni-15Cr-12Al Ni-20Cr-12Al Ni-30Cr-12Al	415.25 407.77 412.51 410.76 414.17	235.08 230.25 231.37 229.04 230.04	347.44 349.60 351.76 359.66 349.93	159.64 171.15 189.88 196.59 200.35	438.02 433.78 438.44 417.25 402.12	210.87 208.76 216.30 207.13 203.73	

			$\ln(a) = -A\tfrac{1}{T} + B$					
				Ni	Cı	:		Al
Alloy Composition	Temperature (K)		$A/10^4$	В	$A/10^{4}$	В	$A/10^{4}$	В
Ni-2Cr-12Al	1423–1636	regression R value (pct)	0.0275 46.1	0.0528	- 0.4922 4.23	- 8.90	1.558 0.9	0.233
Ni-5Cr-12Al	1372–1651	regression R value (pct)	0.0215 48.2	- 0.375	- 0.2779 6.57	- 6.34	1.471 13.4	0.1385
Ni-15Cr-12Al	1445–1652	regression R value (pct)	0.0838 26.9	0.0948	- 0.394 8.81	- 5.16	1.59 0.72	1.082
Ni-20Cr-12Al	1368–1616	regression R value (pct)	0.1478 3.09	0.4241	- 0.399 7.41	- 4.26	1.488 0.35	1.086
Ni-30Cr-12Al	1375–1598	regression R value (pct)	0.1497 3.98	0.2488	-0.3717 8.17	- 3.58	1.096 0.45	- 0.772

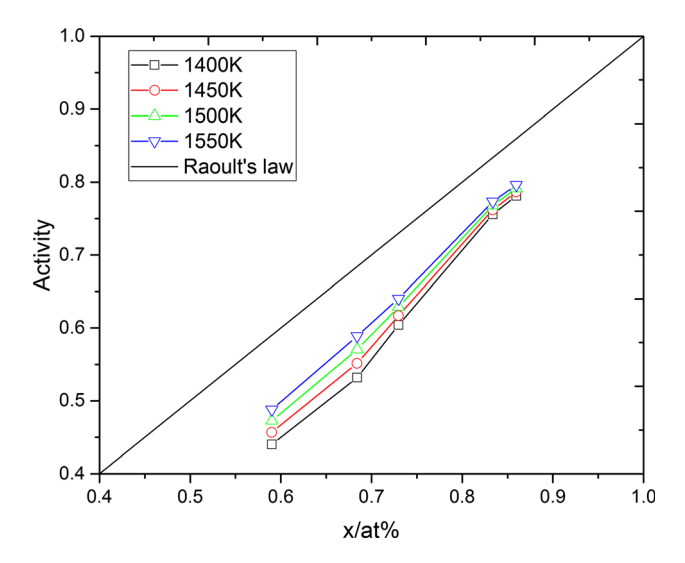


Fig. 8—Activity of Ni vs its atomic fraction in measured Ni-Al-Cr alloys at four temperatures showing negative deviation from ideality of Raoult's law.

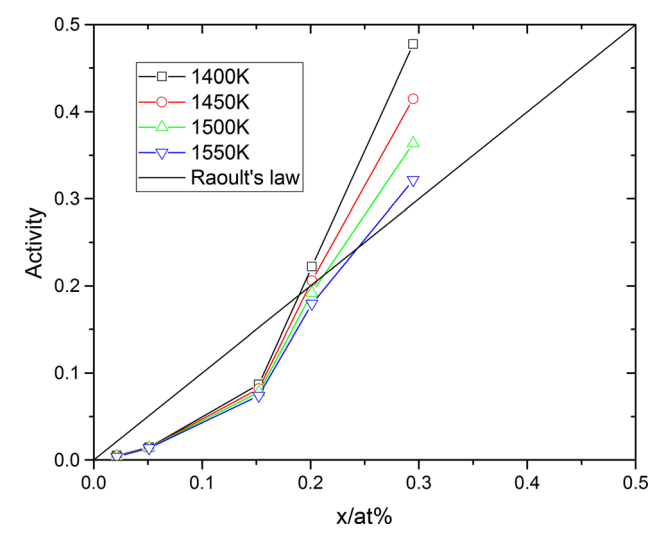
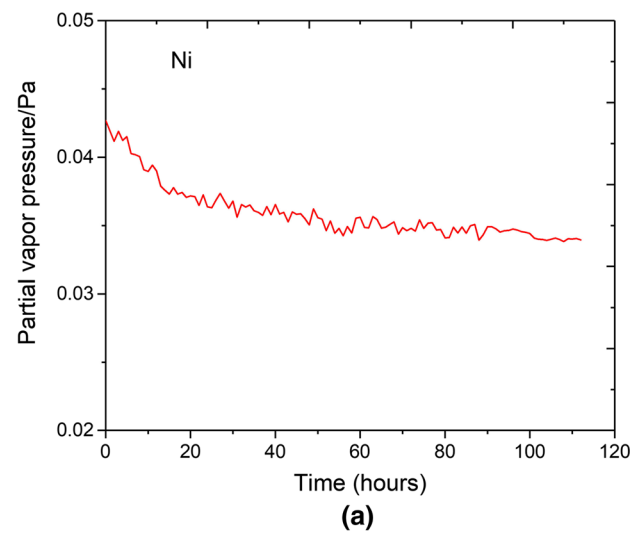


Fig. 9—Activity of Cr vs atomic fraction of Cr in measured Ni-Al-Cr alloys at four temperatures with negative deviation from ideality of Raoult's law.



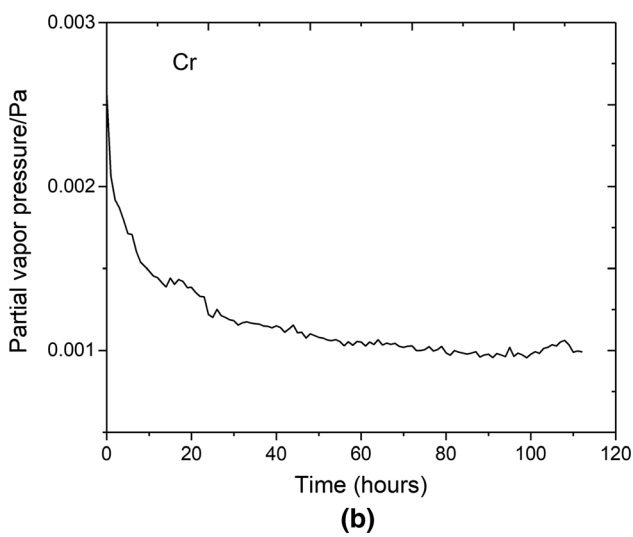


Fig. 10—Variation of partial vapor pressures (Pa) for (a) Ni and (b) Cr in Ni2Cr12Al alloy during the isothermal experiment, showing their contribution to vaporization.

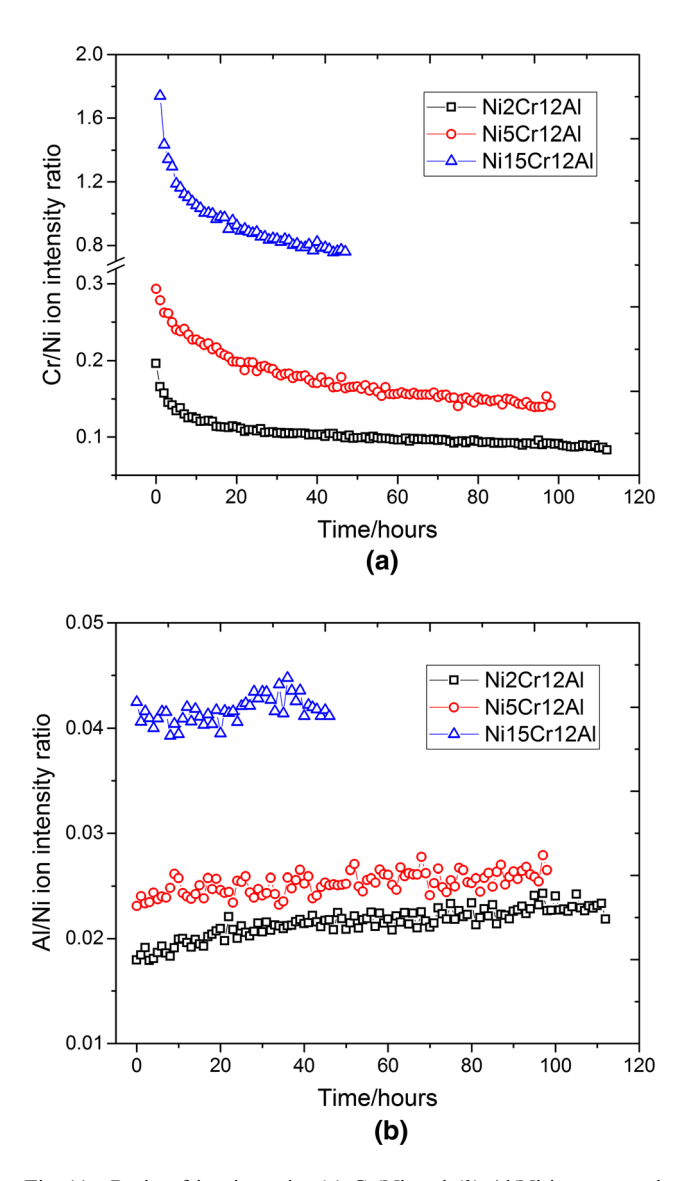


Fig. 11—Ratio of ion intensity (a) Cr/Ni and (b) Al/Ni in measured Ni-Al-Cr alloy during the isothermal experiment, showing the change of elemental concentrations in alloys during isothermal holding.

with re-solving precipitations and loss of the constitution in correlation with the microstructural evolution during solution heat treatment of Ni-base alloys.

V. DISCUSSION

KEMS results have shown the capability of this state-of-the-art technique in quantifying the thermodynamic properties of Ni-Al-Cr alloys, which yield reliable results for activity, partial enthalpy and entropy of formation. KEMS data of measured pure components involved in this study have excellent agreement with the corresponding records from the literature confirming the reproducibility and reliability of current measurements. These novel experimental results provide solid evidence in terms of thermodynamic analysis correlating updated

interpretation of mechanism of vaporization-induced defects in Ni-base superalloys during solution heat treatment.

A. Elemental Vaporization During Casting and Heat Treatment

Vaporization over Ni-base superalloys presumably depends on the thermodynamic properties of elements contained in alloys. Hence, it was assumed that Ni, Al and Cr are major elements contributing to vaporization and inducing phase evolution during solution heat treatment. With respect to the KEMS results, the extent of vaporization in Ni-Al-Cr alloys decisively depends on the amount of Ni and Cr that escapes from the bulk alloys, as illustrated in Figure 5; the order of partial vapor pressures in Ni-base alloys is determined as P_Ni > P_Cr > P_Al. In terms of magnitude, partial vapor pressures of Ni and Cr are at least two orders of magnitude higher than that of Al, indicating the almost negligible amount of Al sublimed from the as-cast alloy. Higher temperature, as a critical factor for vaporization, leads to a steep ascent of the partial vapor pressure for elements in the alloys observed in both Figures 5 and 6. Therefore, the high-temperature behavior of Ni-base alloys is dominated by the stability of the Ni₃Al phase and thermodynamic properties varying with concentrations. Moreover, the disparity of the Cr partial vapor pressure in Figure 6(b) varies by several orders of magnitude in terms of increasing temperature indicating a great tendency of Cr to leave the alloy with sufficient driving force. Similarly, elemental interaction in alloys is mainly driven by the entropy change of Cr, as shown in Table IV.

In addition, Figure 6(c) also shows that the thermodynamic activity of Al in Ni-base alloys is associated with the Cr concentrations showing an ascending trend for Al activity promoted by the local imbalance of Cr concentration. This can be explained by a high-attractive Cr-Ni and low-attractive Cr-Al forces in the alloy compared with the Al-Ni forces, while the attractive Al-Al and Ni-Ni forces remain nearly constant. This means that the bond forces in the alloy support the substitution of Cr for Al in the γ phase and with this a higher volatility of Al, and therefore it is easier for Al atoms to escape from the structure. Consequently, the partial vapor pressure of Al increases with the increase of Cr concentration in the alloy. From another consideration, slow diffusion of Cr in γ phase is related to local segregation of Cr, which leads to enrichment or depletion of Cr at a certain region of alloys that is attributed to the change of Al concentration and activity. Eventually, accumulation of Al in the near surface region promotes the formation of γ' phase as long as the Ni/Al ratio varies locally in a certain portion in Ni-base alloy.

B. Elemental Distribution at Homogenization Stage

From the other aspect, since the KEMS method is always performed in equilibrium state, the experimental results are not restricted to determining the thermodynamic properties of Ni-Cr-Al alloys *via* the derived

equations; KEMS data further show the process of material at high temperatures in reaching equilibrium to reveal the progression of elemental stabilization in terms of KEMS data measured from isothermal holds. Thermodynamic properties of the alloy in its most stable form are critical for predicting the stability of phases and providing optimized parameters used in post-casting processing that prevents defect formation during this stage.

In the case of the initial stage of homogenization as shown in Figure 10, it is considered exothermic enthalpy of formation due to negative deviation from ideality. Cr (52Cr isotope) in the mass spectrometer and its intensity were dependent on the temperature and its phase in the system, while the as-cast Ni-Al-Cr alloys were prepared as the non-equilibrium condition, which shows the process of stabilization at the initial stage of heat treatment. The equilibrium of the sample after casting is insufficient. Cr is either complete in a single face solution or Cr intermetallics. As homogenization continues, Cr migration out of solution and limited solubility in bulk alloys are contributing to decrease the Cr activity in mass spectrometry. Hence, dissolution of Cr in alloys takes longer than that of Al because the preferable substitution of Al with Cr is inhibited by the low activity of Al as a consequence of the longer homogenization time for Cr in Ni-base alloy.

With respect to the supportive experimental result, it permits correlating the KEMS data to understand the mechanism of defect formation during solution heat treatment of Ni-base superalloys providing a view of several unsolved problems.

C. Vaporization-Induced Defects at the Surface Region of Ni-Base Superalloys

Due to the significance of the Ni-Al-Cr system correlating with the investigation of the high-temperature properties of Ni-base superalloys, thermodynamic measurements of Ni-Al-Cr alloys via the KEMS method are able to provide direct and qualitative data revealing elemental interaction during solution heat treatment of Ni-base alloys. Previous microstructural characterization^[27–29] of heat-treated Ni-base superalloys deduced that the morphology of the near surface region evolves from the original substrate γ in the sequence of $\gamma \to \gamma'$ $(Ni_3Al) \rightarrow \beta$ (NiAl), indicating a vaporization-induced microstructural instability during heat treatment, since the depletion of solid-solution elements destabilizes the γ phase and facilitates the formation of a new phase near the surface. However, the difficulty is associated with accurate quantification of elemental vaporization in a solution heat treatment scenario, which requires sufficient data of partial vapor pressures in Ni-base alloys for further assessment of vaporization and interpretation of the mechanism for phase evolution in processing.

Solution heat treatment of most single-crystal superalloys is normally carried out under a low Ar pressure with intermittent purge cycles in practice; therefore, the vaporization of Ni and Cr occurs on the surface of alloys in non-equilibrium condition. Vaporization of Cr during processing is a common phenomenon that has

also been studied in other materials. Lobb and Evans^[62] observed evaporation of elements in stainless steel during vacuum annealing and proposed that the evaporation of Cr occurs through grain boundary migration, which is potentially regarded as a defect of alloys at long annealing times. Li^[63] and Gupta *et al.*^[64] reported the evaporative segregation phenomena in binary Ni-Cr and Fe-Cr alloy, suggesting solute enrichment or depletion in alloys as a result of surface evaporation. As stated by several studies, surface depletion can be a serious problem for a dilute solid alloy^[65,66] leading to microstructural instability of alloys. Semiatin *et al.*^[30] showed principal alloying element loss during high-temperature processing of Ni-base superalloys is Cr in vacuum condition, leading to enrichment of Al at/near the free surface as a consequence of heat treatment.

Sequential evolution of the microstructure in Ni-base superalloys during solution heat treatment is associated with solute redistribution near the surface where a local imbalance of Cr concentration occurs. KEMS data showed fluctuation of partial pressures for Ni and Cr measured in a ternary system deriving a tendency of vaporization for the two elements at high temperatures. Since the site of vaporization is often initiated at the surface, under typical heat treatment conditions, vaporization of Ni in CMSX-10 leads to the decline of the Ni/ Al ratio decomposing profile during solution heat treatment of Ni-base superalloys. Meanwhile, the concentration profile of Cr at the surface is affected by several factors, including diffusivity and vaporization flux. In accordance with the KEMS data in Figures 10 and 11, Cr remains extremely active in Ni-base alloy at high temperature, implying a great tendency of Cr to leave the alloys. The local imbalance of the Cr concentration profile affects the regional equilibrium, which is also associated with diffusion of Al and Cr. In Ni solid solution, the solute transport is diffusion controlled for each element. [30] Therefore, the extent of element diffusion near the surface of the alloy determines the phase that might form during this process. During solution heat treatment, the formation of the phase on the top surface in Ni-base superalloys is associated with enrichment of Al, which is accelerated by the higher concentration profile of Cr at the surface prior to vaporization of Cr. Eventually, the accumulation of Al enriches on the surface, forming as γ' phase. In addition, the degree of Cr vaporization tends to aggravate by the further increase of temperature; therefore, it promotes the growth of the γ' phase layer^[27] and is consistent with the observation of DP in the solution heat treatment window ranging from 1473 K to 1638 K.

In addition, the stabilization of γ' phase is associated with an increase of the Ni/Al ratio or removal with principal solid solute, including Cr. In Figure 11(b), KEMS data during isothermal holds presented as ion intensity ratios of elements confirmed this argument on the effect of phase evolution in Ni-base superalloys despite partial assessment of interactions among three elements that demonstrate certain aspects of the problem. Considering the multiple elements system, variation of the Ni/Al ratio leads to more sophisticated elemental reactions at a high temperature range due to interactions of other

alloying elements influencing the activities of Ni, Al and Cr. Hence, the deduction rationalizes the formation of γ' phase at the surface of Ni-base superalloys during solution heat treatment, which contributes to vaporization-induced defects of alloys. Partial pressures from Ni-Al-Cr alloys referring to the elemental concentration facilitate the improved understanding corresponding to solid experimental evidence from thermodynamic analysis.

D. Implications for Optimization of Heat-Treating Parameters Used in Ni-Base Superalloy Processing

In terms of implications for industrial optimization of heat-treated Ni-base superalloys, the observed kinetic orientation of ion intensity in long-term homogenization of Ni-Al-Cr alloys provides a threshold of solutioning time for dissolution of eutectic phases and segregated dendritic phases. To homogenize the bulk alloy, stabilization of the segregated element can be reflected by the fluctuation of ion intensity in the KEMS results implying at least hours of heat treatment for Ni-base superalloys, which is a potential reference for optimization of the heat treatment parameters involved in current industrial applications. A reliable kinetic timing in solution heat treatment and optimized homogeneous surrounding conditions in terms of temperature equilibrium have a profound effect on reducing casting defects as an effective way during solution heat treatment. Moreover, reconsideration of Al/Ni and Cr/Ni ratios as further optimization of compositional modification prevents the surface from elemental vaporization to improve the thermal stability of Ni-base alloy.

Phase transition in a binary Ni-Al system studied by Hilpert *et al.* [40] has shown transition regions of $\beta + \gamma$ and $\gamma + \gamma'$ for Ni content ranging from 0.7 to 0.72 and 0.76 to 0.8, respectively. However, KEMS data from Ni-Al-Cr alloys have no sufficient scatter points in Figure 8 to further confirm the phase transition for a mole fraction of Ni that varies between 60 to 65 and 72 to 75 at. pct despite a tiny trend of constant Ni activity. Therefore, additional experimental data are required to assess the phase boundaries calculated from the current database, which predicted one phase region for Ni-Al-Cr systems under the temperature range from 1473 K to 1573 K and has to be reviewed.

VI. CONCLUSIONS

Accurate partial vapor pressures of Ni, Al and Cr in Ni-Al-Cr alloys at high temperatures have been determined using the KEMS method. The elemental vaporization during the real industrial solution heat treatment of Ni-base alloys has been analyzed. The following key points can be concluded:

- Accurate partial vapor pressures of Ni, Al and Cr in Ni-base alloys have been obtained from KEMS measurements.
- 2. Partial vapor pressure of Ni and Cr is approximately two orders of magnitude higher than that of

- Al, revealing a great tendency of Ni and Cr to leave the alloy at high temperature, and the vaporization of Al is almost negligible compared with Ni and Cr.
- 3. Partial vapor pressure of Cr in Ni-base alloys declines during the first 20 hours in real industrial heat treatment, and this decrease is due to the inhomogeneity of Cr in the alloy after casting. Therefore, homogenization and vaporization of Cr will be considered in determining a reliable kinetic timing in solution heat treatment to avoid surface defect formation during heat treatment of Ni-base alloys.
- 4. Chromium has a higher resistibility being solved in the alloy than Ni and Al during solution heat treatment. The preferable substitution of Al with Cr is inhibited by the low activity of Al.
- 5. Elemental vaporization occurs during solution heat treatment of Ni-base alloys, which leads to chemistry change, microstructural instability and defect formation at the surface of Ni-base alloys.

ACKNOWLEDGMENTS

The authors acknowledge Professor Wei Liang at Taiyuan University of Technology for preparing Ni–Al–Cr samples and Dr. Elena Yazhenskikh from Forschungszentrum Jülich for support with FactSage data.

OPEN ACCESS

This article is distributed under the terms of the Creative Commons Attribution 4.0 International License (http://creativecommons.org/licenses/by/4.0/), which permits unrestricted use, distribution, and reproduction in any medium, provided you give appropriate credit to the original author(s) and the source, provide a link to the Creative Commons license, and indicate if changes were made.

ELECTRONIC SUPPLEMENTARY MATERIAL

The online version of this article (https://doi.org/10. 1007/s11661-019-05498-1) contains supplementary material, which is available to authorized users.

REFERENCES

- C. Roger: Reed: The Superalloys: Fundamentals and Applications, Cambridge University Press, Cambridge, 2006.
- T.M. Pollock and S. Tin: J. Propul. Power, 2006, vol. 22, pp. 361–74.
- 3. T.M. Pollock: Nat. Mater., 2016, vol. 15, p. 809.

- G.L. Erickson: The Development and Application of CMSX (R)-10, Minerals, Metals and Materials Society, Warrendale, 1996
- N. D'Souza, R. Beanland, C. Hayward, and H.B. Dong: Acta Mater., 2011, vol. 59, pp. 1003–13.
- H.J. Dai, N. D'Souza, and H.B. Dong: Metall. Mater. Trans. A, 2011, vol. 42A, pp. 3430–38.
- H.J. Dai, H.B. Dong, N. D'Souza, J.-C. Gebelin, and R.C. Reed: Metall. Mater. Trans. A, 2011, vol. 42A, pp. 3439–46.
- 8. K. Harris, G.L. Erickson, S.L. Sikkenga, W.D. Brentnall, J.M. Aurrecoechea, and K.G. Kubarych: *J. Mater. Eng. Perform.*, 1993, vol. 2, pp. 481–87.
- A.F. Giamei and D.L. Anton: Metall. Trans. A, 1985, vol. 16, pp. 1997–2005.
- 10. G.L. Erickson: JOM, 1995, vol. 47, pp. 36-39.
- 11. G.E. Fuchs and B.A. Boutwell: *Mater. Sci. Eng. A*, 2002, vol. 333, pp. 72–79.
- N. D'Souza, M. Lekstrom, and H.B. Dong: *Mater. Sci. Eng. A*, 2008, vol. 490, pp. 258–65.
- G.E. Fuchs and M.A. Kaplan: Metall. Mater. Trans. A, 2016, vol. 47A, pp. 2346–61.
- 14. J.W. Aveson, P.A. Tennant, B.J. Foss, B.A. Shollock, H.J. Stone, and N. D'Souza: *Acta Mater.*, 2013, vol. 61, pp. 5162–71.
- M.A. Kaplan and G.E. Fuchs: Metall. Mater. Trans. A, 2016, vol. 47A, pp. 2362–75.
- H.N. Mathur, C. Panwisawas, C. Neil Jones, R.C. Reed, and C.M.F. Rae: Acta Mater., 2017, vol. 129, pp. 112–23.
- 17. G. Brewster, H.B. Dong, N.R. Green, and N. D'Souza: *Metall. Mater. Trans. B*, 2008, vol. 39B, pp. 87–93.
- G. Brewster, N. D'Souza, K.S. Ryder, S. Simmonds, and H.B. Dong: *Metall. Mater. Trans. A*, 2012, vol. 43A, pp. 1288–1302.
- 19. T.M. Pollock: Mater. Sci. Eng. B, 1995, vol. 32, pp. 255-66.
- H.T. Pang, H.B. Dong, R. Beanland, H.J. Stone, C.M.F. Rae, P.A. Midgley, G. Brewster, and N. D'Souza: *Metall. Mater. Trans.* A, 2009, vol. 40A, pp. 1660–69.
- 21. G.E. Fuchs: Mater. Sci. Eng. A, 2001, vol. 300, pp. 52-60.
- N. D'Souza and H.B. Dong: Scripta Mater., 2007, vol. 56, pp. 41–44.
- 23. N. D'Souza and H.B. Dong: *Int. J. Cast Met. Res.*, 2009, vol. 22, pp. 58–61.
- H.T. Pang, N. D'Souza, H. Dong, H.J. Stone, and C.M.F. Rae: *Metall. Mater. Trans. A*, 2016, vol. 47A, pp. 889–906.
- S.L. Semiatin, R.C. Kramb, R.E. Turner, F. Zhang, and M.M. Antony: Scripta Mater., 2004, vol. 51, pp. 491–95.
- 26. H. Wang, N. D'Souza, S. Zhao, D. Welton, N. Warnken, and R.C. Reed: *Scripta Mater.*, 2014, vols. 78–79, pp. 45–48.
- D. Welton, N. D'Souza, J. Kelleher, S. Gardner, Z.H. Dong, G.D. West, and H. Dong: *Metall. Mater. Trans. A*, 2015, vol. 46A, pp. 4298–4315.
- 28. N. D'Souza, S. Simmonds, G.D. West, and H.B. Dong: *Metall. Mater. Trans. A*, 2013, vol. 44A, pp. 4764–73.
- N. D'Souza, D. Welton, G.D. West, I.M. Edmonds, and H. Wang: *Metall. Mater. Trans. A*, 2014, vol. 45A, pp. 5968–81.
- S.L. Semiatin, J.M. Shank, W.M. Saurber, A.L. Pilchak, D.L. Ballard, F. Zhang, and B. Gleeson: *Metall. Mater. Trans. A*, 2014, vol. 45A, pp. 962–79.
- N. D'Souza, D. Welton, J. Kelleher, G.D. West, Z.H. Dong, G. Brewster, and H.B. Dong: in *Superalloys 2016*, Wiley, 2016, pp. 267–77
- 32. K. Hilpert: *Noble Gas and High Temperature Chemistry*, Springer, Berlin, 1990, pp. 97–198.
- 33. K. Hilpert: Fresenius' J. Anal. Chem., 2001, vol. 370, pp. 471-78.
- 34. J. Drowart, C. Chatillon, J. Hastie, and D. Bonnell: *Pure Appl. Chem.*, 2005, vol. 77, pp. 683–737.
- N.C. Oforka and B.B. Argent: J. Less Common Met., 1985, vol. 114, pp. 97–109.
- K. Hilpert and M. Miller: Z. Metallkunde, 1992, vol. 83, pp. 739–43.
- L. Bencze, D.D. Raj, D. Kath, L. Singheiser, K. Hilpert, and W.A. Oates: Metall. Mater. Trans. B, 2004, vol. 35B, pp. 867–76.

- 38. L. Bencze, T. Markus, D. Kath, S. Dash, D.D. Raj, W.A. Oates, W. Löser, and K. Hilpert: *Metall. Mater. Trans. A*, 2006, vol. 37A, pp. 3171–81.
- D. Raj, L. Bencze, D. Kath, W.A. Oates, J. Herrmann, L. Singheiser, and K. Hilpert: *Intermetallics*, 2003, vol. 11, pp. 1119–24.
- K. Hilpert, D. Kobertz, V. Venugopal, M. Miller, H. Gerads, F.J. Bremer, and H. Nickel: Z. Nat. A, 1987, vol. 42, pp. 1327– 32
- 41. K. Hilpert, M. Miller, H. Gerads, and H. Nickel: *Ber. Bunsenges. Phys. Chem.*, 1990, vol. 94, pp. 40–47.
- T. Markus, V. Motalov, D. Kath, and L. Singheiser: in *Proc. Workshop Knudsen Effusion Mass Spectrom.*, N. Jacobson and T. Markus, eds., Electrochemical Soc, Inc., Pennington, 2013, pp. 291–301.
- T. Velikanova, K. Korniyenko, V. Sidorko, and Msit[®] Materials Science International Team: MSI Materials Science International Services GmbH.
- N. Dupin, I. Ansara, and B. Sundman: CALPHAD, 2001, vol. 25, pp. 279–98.
- C.W. Bale, E. Bélisle, P. Chartrand, S.A. Decterov, G. Eriksson, A.E. Gheribi, K. Hack, I.H. Jung, Y.B. Kang, J. Melançon, A.D. Pelton, S. Petersen, C. Robelin, J. Sangster, P. Spencer, and M.A. Van Ende: *CALPHAD*, 2016, vol. 54, pp. 35–53.
- 46. K. Hilpert: J. Electrochem. Soc., 1989, vol. 136, pp. 2099-2108.
- 47. D. Kobertz, M. Müller, and A. Molak: *CALPHAD*, 2014, vol. 46, pp. 62–79.
- 48. Z.H. Dong: A Fundamental Study of Elemental Sublimation During Solution Heat Treatment of Ni-Base Alloys. Ph.D. Thesis, University of Leicester, 2018.
- 49. M. Knudsen: Ann. Phys., 1909, vol. 333, pp. 999-1016.
- 50. K.A. Gingerich: J. Cryst. Growth, 1971, vol. 9, pp. 31-45.
- 51. A. Neckel and S. Wagner: Chem. Mon., 1969, vol. 100, pp. 664-70.
- G.R. Belton and R.J. Fruehan: J. Phys. Chem., 1967, vol. 71, pp. 1403–09.
- J. B. Mann: in Recent Developments in Mass Spectroscopy: Proceedings of the International Conference on Mass Spectroscopy, Kyoto, K. Ogata and H. Teruo, eds., University Park Press, Baltimore, MD, 1970, pp. 814–19.
- M. Berglund and M.E. Wieser: *Pure Appl. Chem.*, 2011, vol. 83, pp. 397–410.
- NIST: Atomic Weights and Isotopic Compositions for All Elements. http://physics.nist.gov/cgi-bin/Compositions/stand_alone.pl, htt p://physics.nist.gov/PhysRefData/Handbook/Tables/nickeltable1. htm. Accessed 01/04/2014.
- F.A. White, T.L. Collins, and F.M. Rourke: *Phys. Rev.*, 1956, vol. 101, pp. 1786–91.
- G.V. Belov, V.S. Iorish, and V.S. Yungman: *CALPHAD*, 1999, vol. 23, pp. 173–80.
- 58. R. Clausius: Ann. Phys., 1850, vol. 155, pp. 500-24.
- 59. É. Clapeyron: J. l'Éc. polytech., 1834, vol. 23, pp. 153–90.
- L.V. Gurvich and I. Veyts: Thermodynamic Properties of Individual Substances: Elements and Compounds, Taylor and Francis, London, 1990.
- 61. Analytical Methods Committee: *Analytical Methods*. AMCTB No. 69, 2015
- 62. R.C. Lobb and H.E. Evans: Met. Sci., 1981, vol. 15, pp. 14-20.
- 63. C.H. Li: Normal Evaporation of Binary Alloys, Grumman Aerospace Corp., Bethpage, NY, 1972.
- K.P. Gupta, J.L. Mukherjee, and C.H. Li: *J. Vac. Sci. Technol.*, 1974, vol. 11, pp. 896–98.
- 65. P.K. Raychaudhuri and F.E. Stafford: *Mater. Sci. Eng.*, 1975, vol. 20, pp. 1–18.
- P.K. Raychaudhuri: Mass Spectrometric and Galvanic Cell Studies of the Thermodynamic Properties of Solid Silver–Palladium Alloys. Ph.D. Thesis, Northwestern University, Ann Arbor, 1971.

Publisher's Note Springer Nature remains neutral with regard to jurisdictional claims in published maps and institutional affiliations.